RESEARCH ARTICLE

Macromolecular Theory and Simulations
www.mts-journal.de

Physical Origin of Distinct Mechanical Properties of Polymer Tethered Graphene Nanosheets Reinforced Polymer Nanocomposites Revealed by Nonequilibrium Molecular Dynamics Simulations

Xu Zhang, Jialiang Chen, and Tianxi Liu*

A non-equilibrium deformation simulation based on standard molecular dynamics is employed to reveal the physical origin of distinct mechanical properties of polymer nanocomposites (PNCs) reinforced by polymer tethered graphene nanosheets (P/G-T). The effect of tethered polymer length (*L*) and interaction strength on the mechanical properties, including tensile stress, modulus, and yield strength, are examined. The simulation results show that the P/G-T systems exhibit improved mechanical properties as *L* and interaction strength increases. The strengthening in attractive interaction between matrix polymer and tethered polymer has a better effect on mechanical properties than that between P and graphene nanosheets. It is found that the bond orientation and nonbonding potential is of crucial importance in determining the mechanical properties of the P/G-T nanocomposite systems. The calculations of radial distribution functions and mean-squared displacement are further performed to reveal the physical origin of enhanced mechanical properties, suggesting that the stronger interfacial interactions will induce the closer packing distance with smaller free volume, higher polymer chain entanglement, and higher restriction of polymer chain movement, which synergistically contribute to the improvement in the mechanical properties. The results may provide useful guidance for promoting the development and practical application of the advanced PNCs with excellent performance.

1. Introduction

Incorporating the nanomaterials into polymer matrices to produce the polymer nanocomposites (PNCs) can endow the polymer materials with various improved properties and functionality,[1,2] such as mechanical,[3,4] thermal,[5,6] electrical,[4,6–8] optical,[9] and rheological[3,10,11] properties thanks to the synergistic effect between the nanomaterials and polymer matrices. Carbon nanomaterial is one kind of widely used nanomaterials as distinct reinforcements for the high-performance PNCs, which has good mechanical properties,[4,12–14] thermal and electrical conductivity,[7,8,13] etc. As "the most marvelous material in 21st century", growing research attention has been paid to graphene as well as its derivatives, which is one-atom-thick 2D layer of sp^2-bonded carbon nanosheet materials, arranged in a honeycomb structure.[15,16] Due to the excellent mechanical, electrically and thermally conductive properties as well as lightweight, there has been an explosion of emphasis on the graphene nanosheets (GN) reinforced PNCs, which show many potential applications in the field of sensors,[17] flexible and wearable devices,[18,19] electrodes,[20,21] electromagnetic interference shielding,[22,23] and other high-performance functional composite materials.[24–27]

However, the self-aggregation of GNs seriously do harm to or even destroy the properties of the final PNCs. Instead of the pristine GNs, the functionalized GNs, decorated by surface modifier through covalently bonding or non-covalent interactions,

X. Zhang, T. Liu
Innovation Center for Textile Science and Technology, State Key Laboratory for Modification of Chemical Fibers and Polymer Materials, College of Materials Science and Engineering
Donghua University
Shanghai 201620, P. R. China
E-mail: xuzhang@dhu.edu.cn

J. Chen
National Garment and Accessories Quality Supervision Testing Center (Fujian), Fujian Provincial Key Laboratory of Textiles Inspection Technology
Fujian Fiber Inspection Center
Fuzhou, Fujian 350026, P. R. China

T. Liu
Key Laboratory of Synthetic and Biological Colloids, Ministry of Education, School of Chemical and Material Engineering
Jiangnan University
Wuxi, Jiangsu 214122, P. R. China

The ORCID identification number(s) for the author(s) of this article can be found under https://doi.org/10.1002/mats.202100044

DOI: 10.1002/mats.202100044

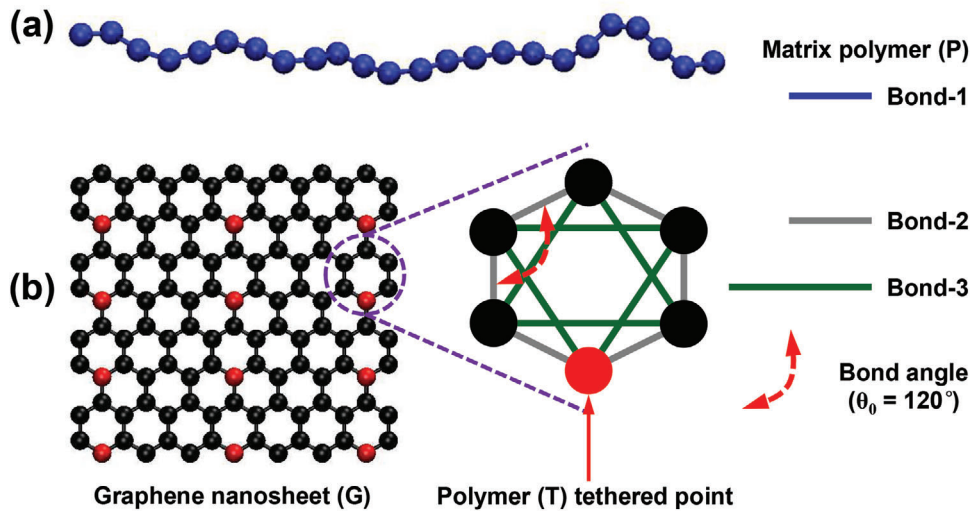

Figure 1. Sketch of the CG model of polymer tethered GNs reinforced PNC (P/G-T) system. a) Linear beads-spring chain model of the flexible matrix polymer. b) Model of surface functionalized GN with 12 tethered points.

are usually produced as nanofillers to improve the immiscibility and dispersion of the GNs in polymer matrices and provide additional functionality for the finally fabricated GNs reinforced PNCs.[14,28–31] The oriented arrangement of GNs and the interaction between GNs and polymers is of crucial importance in determining the performance of all aspects. In the previous work of Pang et al.,[32] the lightweight polyethylene (PE) composite films reinforced with exfoliated thermally reduced graphene oxide (TrGO) fabricated from by using a roll-to-roll hot-drawing process were shown to possess the excellent mechanical properties. The specific ultimate tensile strength and Young's modulus reaches up to 3.2 ± 0.5 and 109.3 ± 12.7 GPa, respectively, with a drawing ratio of 60× and only 1 wt% loading of TrGO, which represent by far the highest reported to date for a polymer/graphene. The employed experimental characterizations and molecular dynamics (MD) simulations revealed that the orientation of the TrGO and the stronger interactions between PE matrix and TrGO than the PE intermolecular (van der Waals) interactions could boost the load transfer from PE matrix to TrGO and take full advantage of the ultrahigh mechanical properties of TrGO. Furthermore, Zhang et al. implemented a non-equilibrium deformation technique based on the dissipative particle dynamics to discover that the hierarchically packed network structure of polymer tethered GNs plays an important role in governing the mechanical properties of the PNCs, which is also found that the strain hardening behaviors, emerged in the PNCs with larger polymer length, mainly benefit from the stretching behaviors of the polymers grafted to GNs.[33]

Despite of the advanced development of PNCs reinforced by GNs both in experiments and theories, it is still room for the theory about how the nature of the surface modifier bonded to GNs influences the mechanical properties. The reinforcing mechanism behind the surface modification of GNs is also not clear. To offset these deficiencies, in the present work, we employed a non-equilibrium deformation simulation based on standard MD to explore the physical origin of distinct mechanical properties of PNCs reinforced by polymer tethered GNs. The effect of tethered polymer length and interaction strength on the mechanical properties was first examined. Based on the calculations of bond orientation and nonbonding potential, the contributions of conformational entropy loss and interaction enthalpy gain to the mechanical properties during the stretch process were clarified. Finally, the radial distribution functions were performed to indicate that the closer packing distance leads to the smaller free volume and effectively restrict the movement of polymer chains, which greatly contributes to the improvement in the mechanical properties. The simulation results may provide useful guidance for designing and preparing high-performance PNCs as well as other advanced polymer matrix composite materials.

2. Experimental Section

2.1. Coarse-Grained Molecular Dynamics

A coarse-grained (CG) model of polymer tethered GNs reinforced PNC (P/G-T) system was constructed, as illustrated in **Figure 1**. In the present CG model, a bead represents a cluster of atoms, involving plenty of repeat units. The matrix polymer (denoted by P, Figure 1a) is modelled by a linear beads-spring chain consisting of L_p beads linked by L_p-1 bonds (Bond-1, the blue lines in Figure 1a). Each GN (denoted by G, Figure 1b), containing N_G = 120 beads connected by bonds (Bond-2, the dark gray lines in Figure 1b), have 12 functional points (Figure 1b, i.e., surface functionalized by 10%) to tether the surface-modifier polymer T. Like the matrix polymer (P), the polymer (T) tethered to GN (G) is also mimicked as a linear bead-spring chain consisting of L beads linked by L bonds (Bond-1, the first bond is tethered to the polymer tethered point on GN marked by a red arrow in Figure 1b), which is omitted in Figure 1. The mass and diameter of each polymer and GN bead is set to be m and σ. To make the model of GN (G) more reasonable, another kind of bonds (Bond-3, the olive lines in Figure 1b) and the bond angles (denoted by θ_0, indicated by the red arc in Figure 1b) were also introduced into the model.[33] In according to the hexagonal structure of graphene,

the bond angle (θ_0) of Bond-2, the bond length of Bond-2 (l_{b2}) and Bond-3 (l_{b3}) must satisfy[33]

$$\theta_0 = 120^\circ \tag{1}$$

$$l_{b3} = \sqrt{3} l_{b2} \tag{2}$$

In general, for the CG simulations of polymer and carbon materials, both the CG bond and angle potentials should be considered.[34] Herein, the considered polymers, including P and T, are modelled as flexible or coil chains, and therefore, the angle potentials of the polymer chains vanished and were not considered. However, the angle potentials of the GNs could not be omitted and would be discussed in the following. It is notable that the CG hexagonal structures in Figure 1b do not correspond to the carbon hexagonal structures in the GNs due to the fact that one CG bead represents a cluster of carbon atoms in the GNs. Actually, there are many feasible CG strategies for the GNs or other kind of sheet-shaped nanofillers based on the single regular polygon patterns,[10,33] known as (3^6), (4^4), and (6^3) Archimedean tiling patterns.[35,36] In the present CG model, the simplest and most reasonable pattern with regular hexagons were selected to effectively mimic the structural, bendable, and foldable nature of the GNs tailored by the two kinds of bond potentials (Bond-2 and Bond-3) and the angle potentials of Bond-2.[33]

In the present MD simulations, the interaction potential includes the nonbonding potential U_{ij} and bonding potential U_{bond}. The nonbonding potential U_{ij} is given by the modified Lennard–Jones 12:6 (LJ126) potential acting between any pair of ith and jth beads

$$U_{ij} = \begin{cases} 4\epsilon_{ij}\left[\left(\frac{\sigma}{r_{ij}}\right)^{12} - \left(\frac{\sigma}{r_{ij}}\right)^{6} - \left(\frac{\sigma}{r_{ij}{}^{c}}\right)^{12} + \left(\frac{\sigma}{r_{ij}{}^{c}}\right)^{6}\right], & r_{ij} \le r_{ij}{}^{c} \\ 0, & r_{ij} > r_{ij}{}^{c} \end{cases} \tag{3}$$

where the ϵ_{ij} is the interaction parameter between beads i and j. The $r_{ij}{}^{c}$ is the cutoff distance for r_{ij} at which the potential is truncated and shifted to yield zero energy and force. In the modified LJ126 potential, the cutoff distance ($r_{ij}{}^{c}$) determines the attractive ($r_{ij}{}^{c} > 2^{1/6}\sigma$) or repulsive ($r_{ij}{}^{c} \le 2^{1/6}\sigma$) interaction between i and j beads, where the σ represents the distance unit in the MD simulations. To prevent the GNs from aggregation, the cutoff distance is set to be $2^{1/6}\sigma$ (repulsive) for the G–G and G–T interaction, that is, $r_{GG}{}^{c} = r_{GT}{}^{c} = 2^{1/6}\sigma$. The cutoff distance for P–P, P–G, P–T, and T–T interaction is fixed at 2.5σ (attractive). For convenience and clearness, we use the superscript of positive (+) and negative (−) sign for the interaction strength parameter ($\epsilon_{ij}{}^{+}$ or $\epsilon_{ij}{}^{-}$) to describe the repulsive and attractive interaction between i and j beads. In the present work, the length of matrix polymer L_P is set to be 24 without changing, while the interaction strength of G–G, P–P, and T–T is fixed at 1.0ϵ, that is, $\epsilon_{GG}{}^{+} = 1.0\epsilon$, $\epsilon_{PP}{}^{-} = 1.0\epsilon$, and $\epsilon_{TT}{}^{-} = 1.0\epsilon$, where the ϵ represents the unit of energy in the MD simulations. The length of tethered polymer (L) and the interaction strength parameters ($\epsilon_{GT}{}^{+}$, $\epsilon_{PG}{}^{-}$, and $\epsilon_{PT}{}^{-}$) are variable.

The bonding potential U_{bond} is given by the modified finite extensible nonlinear elastic potential

$$U_{bond} = -0.5 k_b R_0{}^2 ln\left[1 - \left(\frac{r}{R_0}\right)^2\right] \tag{4}$$

where $k_b = 20\epsilon/\sigma^2$ and $R_0 = 1.5\sigma$ (for Bond-1 and Bond-2) or 2.5σ (for Bond-3) is the elastic coefficient and the maximum extensible bond length, respectively. A cosine harmonic function (angle potential) was used to further constrain the hexagonal structure of graphene, written as

$$U_{angle}(\theta) = \frac{1}{2} k_a (cos\theta - cos\theta_0)^2 \tag{5}$$

where $k_a = 50\epsilon$ is the angle spring constant and $\theta_0 = 120^\circ$ is the equilibrium angle.

In the present work, the total number of CG MD beads was fixed at 12 000, containing 10 nanosheets of polymer tethered graphene (each GN includes $N_G = 120$ beads, that is, the mass fraction of GNs in the P/G-T nanocomposite systems was $10N_G/12\,000 \times 100\% = 10\%$). All the MD simulations were carried out by the large scale atomic/molecular massively parallel simulator, developed by Sandia National Laboratories.[37] In the MD simulations, to generate the initial configurations, a large system was constructed with low volume fraction, which was compressed to the volume fraction of 0.45. Based on the initial configurations, the MD simulations were performed in the isothermal-isobaric (NPT) ensemble by using the Nose–Hoover barostat and thermostat. During the MD simulations, the periodic boundary conditions were imposed with a time step $\Delta t = 0.004\tau$ (τ denotes the unit time).

2.2. Nonequilibrium Simulation

The nonequilibrium deformation technique based on the standard MD method (NEMD) were implemented to simulate the tensile behaviors of the P/G-T nanocomposite systems after enough equilibration (10^7 MD simulation steps) subject to a uniaxial deformation on the MD simulation box along the z direction under the NVT ensemble with $T = 1.0$ and $\Delta t = 0.001\tau$. As the box is elongated in the z direction, the box lengths in the x and y directions are changed simultaneously to keep the system volume constant. To make sure more physical sense, the simulated P/G-T nanocomposite systems are assumed to have no volume change and incompressible, and the Poisson's ratio μ is set to be 0.5. The uniaxial deformation occurs over the period of 100τ and the strain rate is set as $0.0327/\tau$. For the assemble average of stress, eleven tension tests were performed based on the equilibrated structures and dynamics data collected from the last 10^5 MD simulation steps at every 10^4 steps. The more details of MD model, MD simulations, and NEMD method can be found in the former reported works.[10,11,38]

3. Results and Discussion

First, we examined the effect of L (the length of tethered polymer) and $\epsilon_{GT}{}^{+}$ (the strength of repulsive interaction between G

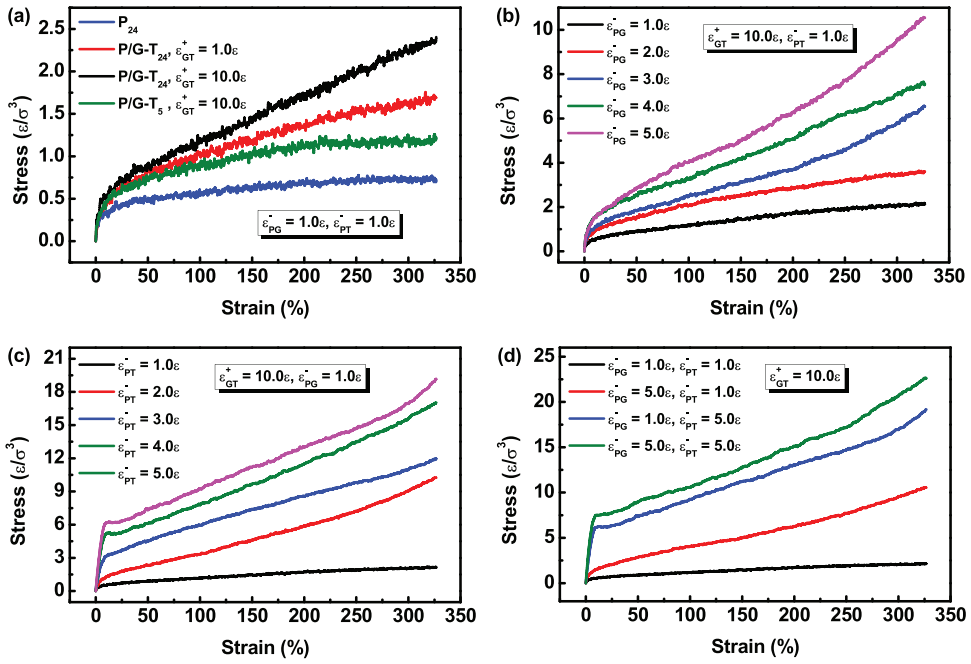

Figure 2. a) Tensile properties of the pure homopolymer (P_{24}) and polymer tethered GN reinforced PNC (P/G-T_L) systems with different tethered polymer lengths ($L = 24$ or 5) and repulsive interaction strengths ($\epsilon_{GT}{}^{+} = 1.0\epsilon$ or 10.0ϵ). Effect of the attractive interaction strength of a) P-G ($\epsilon_{PG}{}^{-}$), b) P-T ($\epsilon_{PT}{}^{-}$), and c) comparison of the $\epsilon_{PG}{}^{-}$ and $\epsilon_{PT}{}^{-}$ on the tensile properties of the P/G-T nanocomposite systems with $L = 24$ and $\epsilon_{GT}{}^{+} = 10.0\epsilon$.

and T) on the tensile properties of P/G-T_L nanocomposite systems, as presented in **Figure 2**a. As a comparison, a model of pure homopolymer with 24 beads (P_{24}) was also constructed, where the cutoff distance and repulsive interaction are corresponding to the matrix polymer (P) in the P/G-T nanocomposite systems, which is 2.5σ (attractive) and 1.0ϵ, respectively. In general, the P/G-T nanocomposite systems show a relative higher stress than the pure polymeric system (P_{24}, the blue curve in Figure 2a) at the same strain, suggesting that the simulated P/G-T nanocomposite systems possess the better mechanical properties than the pure polymeric system. For the interaction parameter ($\epsilon_{GT}{}^{+}$), the stronger repulsive interaction between G and T produces the higher tensile stress at the same strain (the red curve with $\epsilon_{GT}{}^{+} = 1.0\epsilon$ and the black curve with $\epsilon_{GT}{}^{+} = 10.0\epsilon$ in Figure 2a), which is also revealed in the nanoparticle tethering polymers.[11,37] In addition, the length of tethered polymer (L) on GN unquestionably shows an important role in determining the mechanical properties of the P/G-T nanocomposite systems, comparing the red curve (larger $L = 24$) with the olive curve (smaller $L = 5$). In the present work, the primary purpose is to clarify the effect of reinforcements (including the tethered polymers and the GNs) on the mechanical properties of the P/G-T nanocomposite systems. Therefore, in the following study, we just focus on the P/G-T nanocomposite systems with better mechanical properties at fixed $L = 24$ and $\epsilon_{GT}{}^{+} = 10.0\epsilon$.

Figure 2b–d display the effect of the attractive interaction strength ($\epsilon_{PG}{}^{-}$ and $\epsilon_{PT}{}^{-}$) on the mechanical properties of the P/G-T nanocomposite systems with $L = 24$ and $\epsilon_{GT}{}^{+} = 10.0\epsilon$. As shown in Figure 2b (or Figure 2c), the tensile stress increases as the $\epsilon_{PG}{}^{-}$ (or $\epsilon_{PT}{}^{-}$) increases at the same strain, indicating that the increase in the strength of attractive interaction between matrix polymer P and GNs G (or tethered polymer T) could effectively improve the mechanical properties of the P/G-T nanocomposite systems. For the strength of attractive interaction between matrix polymer (P) and tethered polymer (T), it can be further seen from Figure 2c (at smaller strain < 10%) that the tensile modulus of the P/G-T nanocomposite systems dramatically increases as the $\epsilon_{PT}{}^{-}$ increases. The detail information about the tensile modulus would be discussed later. Shown in Figure 2d is the comparison of the effect of $\epsilon_{PG}{}^{-}$ and $\epsilon_{PT}{}^{-}$ on the tensile behaviors of the P/G-T nanocomposite systems, which demonstrates that the strengthening in the attractive interaction between matrix polymer and tethered polymer ($\epsilon_{PT}{}^{-}$, the blue and olive cures in Figure 2d) has a better effect on the mechanical properties (including the tensile stress and modulus) compared to the increase in the attractive interaction between matrix polymer and GNs ($\epsilon_{PG}{}^{-}$, the black and red curves in Figure 2d).

To further examine the effect of the attractive interaction strength between matrix polymer and tethered polymer ($\epsilon_{PT}{}^{-}$), the tensile behaviors of the P/G-T nanocomposite systems with $L = 24$, $\epsilon_{GT}{}^{+} = 10.0\epsilon$, and $\epsilon_{PG}{}^{-} = 3.0\epsilon$ (the middle attractive interaction strength between matrix polymer and GNs) was investigated, as embedded in **Figure 3**. It can be seen from Figure 3a that as the $\epsilon_{PT}{}^{-}$ increases, the stress at the same strain increases rapidly, which becomes more markedly at relative larger strain region. The stress–strain relationship or tensile behavior is more complicated at smaller strain region than larger strain region. At smaller strain region, the stress–strain curves show a common character (elastic behavior) that the tensile stress increases approximately linearly, indicating that the P/G-T nanocomposite systems can be considered as an ideal elastomer at lower strain region. By the linear fitting of the stress–strain curve within 2.0% strain, the tensile modulus could be obtained and was found to increase with increasing the $\epsilon_{PT}{}^{-}$, as shown in Figure 3b. It suggests that

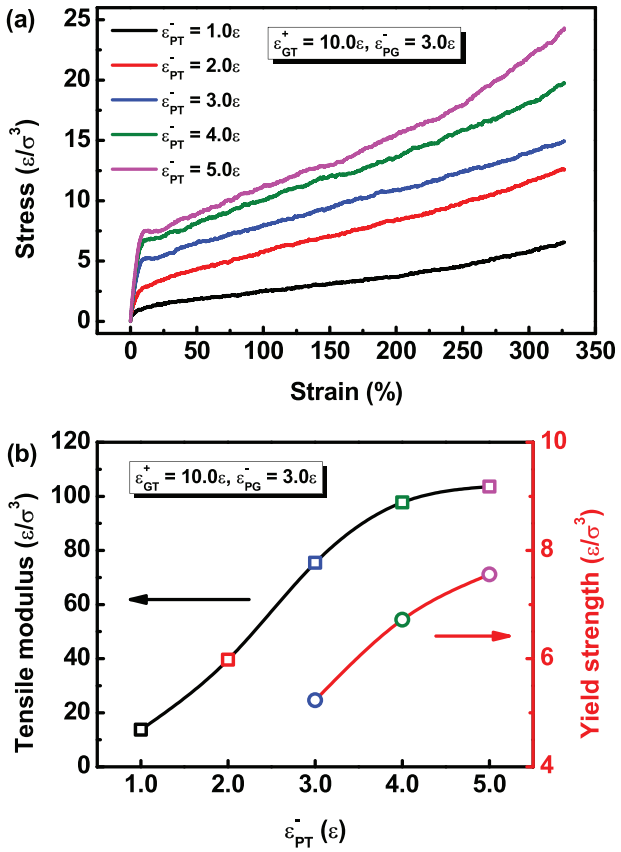

Figure 3. Effect of the attractive interaction strength of P-T (ϵ_{PT}^-) on the tensile properties of the P/G-T nanocomposite systems with $L = 24$, $\epsilon_{GT}^+ = 10.0\epsilon$, and $\epsilon_{PG}^- = 3.0\epsilon$: a) stress–strain relationship; b) tensile modulus and yield strength versus ϵ_{PT}^- calculated from (a).

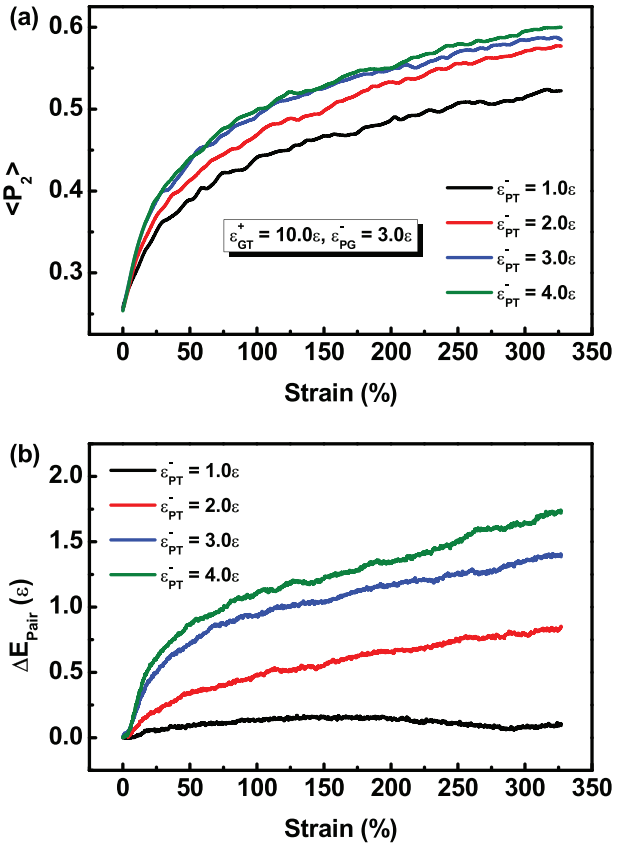

Figure 4. a) Order parameter $<P_2>$ of bond orientation for matrix polymer and b) changes of nonbonding potential ΔE_{pair} between deformed and undeformed states with respect to the strain during the stretching process of the P/G-T nanocomposite systems at various ϵ_{PT}^- with $\epsilon_{GT}^+ = 10.0\epsilon$ and $\epsilon_{PG}^- = 3.0\epsilon$.

the tethered polymer (T) with greater affinity for the matrix polymer (P) shows a more superior effect on enhancing the P/G-T nanocomposite systems. In addition to the elastic behavior, the yield behavior with obvious and well-defined yield point occurs in the stress–strain curve at low strain region with larger ϵ_{PT}^- (e.g., $\epsilon_{PT}^- = 3.0\epsilon$, 4.0ϵ, and 5.0ϵ, corresponding to the blue, olive, and magenta stress–strain curve in Figure 3a, respectively), while the yield phenomenon is unobvious with smaller ϵ_{PT}^- (e.g., $\epsilon_{PT}^- = 1.0\epsilon$ and 2.0ϵ, corresponding to the black and red stress–strain curve in Figure 3a, respectively). The plot of yield strength (the stress at yield point in Figure 3a) with respect to ϵ_{PT}^- from 3.0ϵ to 5.0ϵ was presented in Figure 3b. As can be seen form Figure 3b, the yield strength shifts up to higher value with strengthening the attractive interaction between matrix polymer (P) and tethered polymer (T), ϵ_{PT}^-.

To get a deep insight into the influencing mechanisms of the polymer tethered GNs on the tensile stress–strain behaviors, the order parameter of bond orientation for matrix polymer (P) and nonbonding potential during the stretching process were further examined, as illustrated in **Figure 4**a,b, respectively. The order parameter of bond orientation was characterized by the second-order Legendre polynomials $<P_2> = (3<\cos^2\theta>-1)/2$, reflecting the chain alignment along the deformed direction, where the θ is the angle between bonds and deformed direction. As shown in Figure 4a, the order parameter $<P_2>$ of matrix polymer (P) shifts upward (increases) as the ϵ_{PT}^- increases at any equal strain for the smaller ϵ_{PT}^- (e.g., $\epsilon_{PT}^- = 1.0\epsilon$, 2.0ϵ, and 3.0ϵ), while the $<P_2>$ shows slightly affected by the ϵ_{PT}^- as it become larger. For instance, the curve of $<P_2>$ versus strain for $\epsilon_{PT}^- = 4.0\epsilon$ (the olive curve in Figure 4a) is almost overlapped with the curve for $\epsilon_{PT}^- = 3.0\epsilon$ (the blue curve in Figure 4a).

Usually, the generated tensional stress arises from the loss of conformational entropy and the increase of interaction enthalpy.[39,40] The bond orientation (measured by $<P_2>$) only contribute to the tensile stress in terms of the conformational entropy loss. The increase in interaction enthalpy can be embodied by the change of nonbonding potential ΔE_{pair} during the stretching process, which is the difference of overall nonbonding potentials between deformed and undeformed states. The variation of ΔE_{pair} as a function of strain at various ϵ_{PT}^- during the stretching process was placed in Figure 4b. It is can be convinced from Figure 4b that the ΔE_{pair} becomes larger when the ϵ_{PT}^- is larger, implying that the nonbonding potential interactions make greater contributions to the tensile stress at larger ϵ_{PT}^- during the stretching process. Note that the higher bond stretching (orientation) results in the larger conformational entropy loss and the larger nonbonding potential increment leads to the

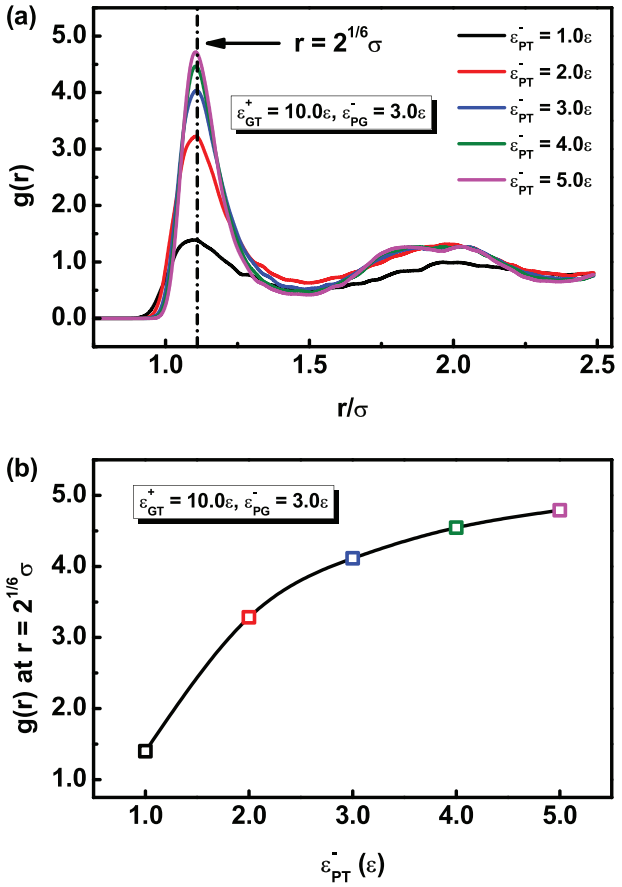

Figure 5. a) Radial distribution functions $g(r)$ between matrix polymer (P) and tethered polymer (T) for the P/G-T nanocomposite systems at various $\epsilon_{PT}{}^{-}$ with $\epsilon_{GT}{}^{+} = 10.0\epsilon$ and $\epsilon_{PG}{}^{-} = 3.0\epsilon$. b) The $g(r)$ value at the prominent peak ($r = 2^{1/6}\sigma$) as a function of $\epsilon_{PT}{}^{-}$ obtained from (a).

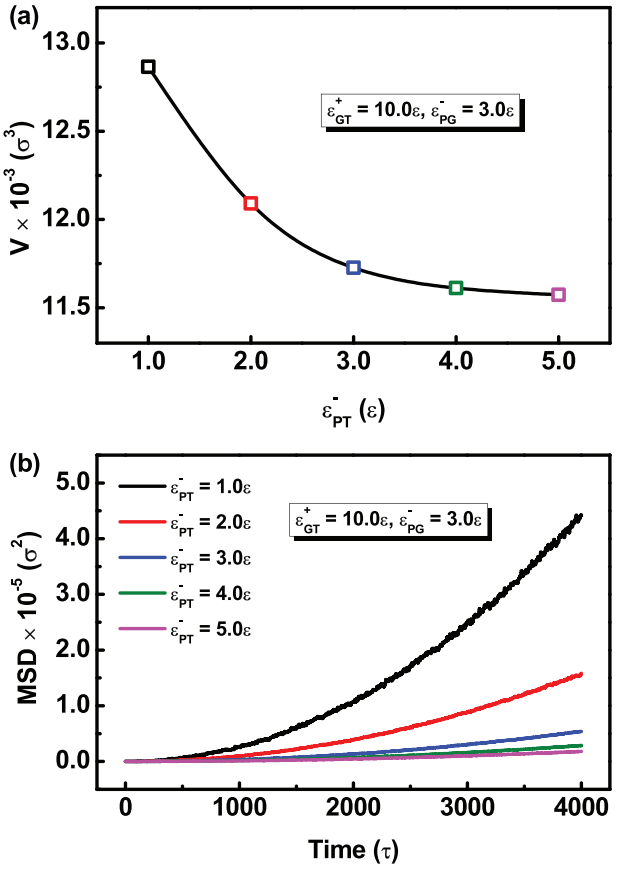

Figure 6. Plot of a) total volume V as a function of $\epsilon_{PT}{}^{-}$ and b) MSD as a function of time for the matrix polymer (P) at various $\epsilon_{PT}{}^{-}$ with $\epsilon_{GT}{}^{+} = 10.0\epsilon$ and $\epsilon_{PG}{}^{-} = 3.0\epsilon$.

larger interaction enthalpy gain. Under the synergistic action of enthalpy and entropy, the polymer tethered GNs reinforced PNC systems possess the higher tensile stress (Figures 2 and 3), modulus (Figure 3b), and yield stress (Figure 3b) at stronger attractive interaction between matrix polymer and tethered polymer, $\epsilon_{PT}{}^{-}$. It can also be concluded and predicted that the greater enhancement effect on mechanical properties of the P/G-T nanocomposite systems can also be observed at stronger attractive interaction between matrix polymer and GNs, $\epsilon_{PG}{}^{-}$, as preliminarily resulted in Figure 2b.

On behalf of deep insight into the physical origin of the enhanced mechanical properties of the P/G-T nanocomposite systems with larger $\epsilon_{PT}{}^{-}$ (the stronger attraction between matrix polymer and tethered polymer), the radial distribution functions $g(r)$ between matrix polymer (P) and tethered polymer (T) for the P/G-T nanocomposite systems at various $\epsilon_{PT}{}^{-}$ were performed, as shown in **Figure 5**. The radial distribution function, $g(r)$, also called pair distribution function or pair correlation function, is an important structural characteristic, which represents the probability to find an atom in a shell dr at the distance r of another atom chosen as a reference point. The peak position and intensity of typical peaks in g(r) can determine the packing geometry.[41,42] For all the P/G-T nanocomposite systems, the $g(r)$ plots show a prominent peak at the equilibrium distance ($r = 2^{1/6}\sigma$), suggesting that a large number of tethered polymers directly contact with matrix polymers. The $g(r)$ peak intensity increases significantly as the $\epsilon_{PT}{}^{-}$ increases from 1.0ϵ to 5.0ϵ, as presented in Figure 5b. This indicates that the matrix polymers are closer to the tethered polymers leading to a better reinforcement (polymer tethered GN, G-T) dispersion in the P/G-T nanocomposite systems and the stronger attractive interaction.[42] Moreover, the closer packing distance between matrix polymers and tethered polymers induces the smaller free volume and would effectively restrict the movement of polymer chains, which makes great contributions to the improvement in the mechanical properties including the tensile stress and modulus, etc.

For more intuitively, the calculations of the total volume and the mean-squared displacement (MSD) were also supplemented to show that the free volume are reduced and the movement of polymer chains are restricted with the increase of $\epsilon_{PT}{}^{-}$, respectively, as presented in **Figure 6**. The total volume, $V = V_0 + V_f$, as a function of $\epsilon_{PT}{}^{-}$ was plotted in Figure 6a, which shows a decrease as the $\epsilon_{PT}{}^{-}$ increases, indicating that the free volume (V_f) decreases due to that the excluded volume (V_0) of the P/G-T nanocomposite system is fixed without changing. The temporal evolution of the MSD as a function of time for the matrix polymer (P) at various $\epsilon_{PT}{}^{-}$ was presented in Figure 6b,

which was obtained from the MD simulations at the equilibrium state through MSD = $[R(t) - R(0)]^2$, where the $R(t)$ and $R(0)$ is the position of center-of-mass of MD atoms at time t and 0, respectively.[43] It can be seen from Figure 6b that the value of MSD decreases as the $\epsilon_{PT}{}^{-}$ increases at the same time (t), suggesting that stronger attraction between P and T (larger $\epsilon_{PT}{}^{-}$) would effectively restrict the mobility of the matrix polymer chains to improve the above-mentioned mechanical properties.

Before leaving this section, we would like to remark on the effect of the polymer chain entanglement or winding on the mechanical properties of the P/G-T nanocomposite systems. It is well known that the interfacial strength between matrix and reinforcements play a key role in determining the mechanical properties of the composite systems. In the studied P/G-T nanocomposite systems, the interfacial strength should be divided into two parts: the nonbonding interactions (LJ potentials, i.e., ΔE_{pair} in Figure 4b, as mentioned above)[44] and polymer chain entanglement or winding (i.e., mechanical interlock). The mechanical interlock between P and T has a great influence on the interfacial strength. In the presented MD simulations, we could not characterize the polymer chain entanglement directly. However, the polymer chain entanglement could be indirectly reflected by the $<P_2>$ and the polymer chain mobility, where the higher degree of polymer chain entanglement leads to higher value of $<P_2>$ at the same strain (Figure 4a) and higher restriction of polymer chain movement (i.e., lower value of MSD at the same time, as shown in Figure 6b). In these aspects, the increase in the interfacial strength ($\epsilon_{PT}{}^{-}$) would result in the higher degree of mechanical interlock between P and T, which makes contributions to the mechanical properties.

Overall, the present MD simulation results revealed the physical principles of distinct mechanical properties of the PNCs reinforced by polymer tethered GNs and may provide useful information for designing and preparing advanced PNC materials with excellent performance. However, it still remains a room for further discovery both in fundamental and applied study in nanosheet-reinforced PNC materials, such as compressive properties, viscoelasticity, thermal and electrical properties, as well as the mechanism behind the modification and improvement, etc., which are all worthy of being demonstrated to promote the development and practical application of the advanced PNC materials.

4. Conclusions

In the present work, we employed the non-equilibrium deformation technique based on the standard MD (NEMD) to reveal the physical origin of distinct mechanical properties of the PNCs reinforced by polymer tethered GNs (P/G-T). The tethered polymer length (L) and interaction strength play important roles in improving the tensile properties, including tensile stress, modulus, and yield strength, showing that the P/G-T nanocomposite systems exhibit improved tensile properties as the L and the interaction strength increases. The increase in the attractive interaction strength between matrix polymer (P) and tethered polymer (T) has a better effect on mechanical properties than that between P and GN in the P/G-T nanocomposite systems. It was convinced that the bond orientation and nonbonding potential is of crucial importance in determining the mechanical properties of the P/G-T nanocomposite systems. Finally, it was also found that the stronger interfacial interactions would induce the closer packing distance with smaller free volume, higher polymer chain entanglement, and higher restriction of polymer chain movement, which synergistically make great contributions to the improvement in the mechanical properties of the P/G-T nanocomposite systems. The results obtained from these simulations may provide useful guidance for designing and preparing high-performance PNCs as well as other advanced polymer matrix composite materials.

Acknowledgements

This work was supported by the Natural Science Foundation of Shanghai (Grant No.: 21ZR1402800), the Fundamental Research Funds for the Central Universities (Grant No.: 2232020D-11), the China Postdoctoral Science Foundation (Grant No.: 2021M690597), and the Open Project Program of Fujian Provincial Key Laboratory of Textiles Inspection Technology (Fujian Fiber Inspection Center) (Grant No.: 2020-MXJ-04).

Conflict of Interest

The authors declare no conflict of interest.

Data Availability Statement

Research data are not shared.

Keywords

graphene nanosheets, mechanical properties, molecular dynamics, nonequilibrium simulations, polymer nanocomposites

Received: June 24, 2021
Revised: August 10, 2021
Published online: August 19, 2021

[1] V. Unnikrishnan, O. Zabihi, M. Ahmadi, Q. Li, P. Blanchard, A. Kiziltas, M. Naebe, *J. Mater. Chem. A* **2021**, *9*, 4348.
[2] Z. Zheng, X. Xia, X. Zeng, X. Li, Y. Wu, J. Liu, L. Zhang, *Macromol. Rapid Commun.* **2018**, *39*, 1800382.
[3] A. S. Pakdel, E. Niinivaara, E. D. Cranston, R. M. Berry, M. A. Dubé, *Macromol. Rapid Commun.* **2020**, *42*, 2000448.
[4] V. Agarwal, Y. Fadil, A. Wan, N. Maslekar, B. N. Tran, R. A. Mat Noor, S. Bhattacharyya, J. Biazik, S. Lim, P. B. Zetterlund, *ACS Appl. Mater. Interfaces* **2021**, *13*, 18338.
[5] J. Wang, S. Mubarak, D. Dhamodharan, N. Divakaran, L. Wu, X. Zhang, *Compos. Commun.* **2020**, *19*, 142.
[6] Y. Zheng, R. Wang, X. Dong, L. Wu, X. Zhang, *ACS Appl. Mater. Interfaces* **2018**, *10*, 28103.
[7] A. Z. Yazdi, I. O. Navas, A. Abouelmagd, U. Sundararaj, *Macromol. Rapid Commun.* **2017**, *38*, 1700176.
[8] J. Payandehpeyman, M. Mazaheri, M. Khamehchi, *Compos. Commun.* **2020**, *21*, 100364.
[9] T. Zhou, G. Wan, X. Kong, B. Li, L. Wu, *Macromol. Rapid Commun.* **2020**, *41*, 2000468.
[10] W. Hong, J. Lin, X. Tian, L. Wang, *J. Phys. Chem. B* **2020**, *124*, 6437.
[11] P. Xu, J. Lin, L. Zhang, *J. Phys. Chem. C* **2017**, *121*, 28194.

[12] M. Wang, L. Ma, B. Li, W. Zhang, H. Zheng, G. Wu, Y. Huang, G. Song, *Compos. Commun.* **2020**, *22*, 100514.
[13] B. Dey, M. W. Ahmad, A. Almezeni, G. Sarkhel, D. S. Bag, A. Choudhury, *Compos. Commun.* **2020**, *17*, 87.
[14] L. Zhang, R. Wang, J. Wang, L. Wu, X. Zhang, *Nanoscale* **2019**, *11*, 2343.
[15] A. K. Geim, A. H. MacDonald, *Phys. Today* **2007**, *60*, 35.
[16] Y. Si, E. T. Samulski, *Nano Lett.* **2008**, *8*, 1679.
[17] R. Wang, Z. Tan, W. Zhong, K. Liu, M. Li, Y. Chen, W. Wang, D. Wang, *Compos. Commun.* **2020**, *22*, 100426.
[18] S. K. Kim, T. Ha, C. Lee, H. Chang, H. D. Jang, *Macromol. Rapid Commun.* **2019**, *40*, 1800832.
[19] Y. Guo, J. Xu, W. Wu, S. Liu, J. Zhao, E. Pawlikowska, M. Szafran, F. Gao, *Compos. Commun.* **2020**, *22*, 100542.
[20] W. Alkarmo, F. Ouhib, A. Aqil, J.-M. Thomassin, J. Yuan, J. Gong, B. Vertruyen, C. Detrembleur, C. Jérôme, *Macromol. Rapid Commun.* **2018**, *40*, 1800545.
[21] D.-W. Wang, F. Li, J. Zhao, W. Ren, Z.-G. Chen, J. Tan, Z.-S. Wu, I. Gentle, G. Q. Lu, H.-M. Cheng, *ACS Nano* **2009**, *3*, 1745.
[22] Q. Jiang, X. Liao, J. Yang, G. Wang, J. Chen, C. Tian, G. Li, *Compos. Commun.* **2020**, *21*, 100416.
[23] Z. Chen, C. Xu, C. Ma, W. Ren, H.-M. Cheng, *Adv. Mater.* **2013**, *25*, 1296.
[24] H.-P. Cong, X.-C. Ren, P. Wang, S.-H. Yu, *Energy Environ. Sci.* **2013**, *6*, 1185.
[25] R. Shu, J. Zhang, C. Guo, Y. Wu, Z. Wan, J. Shi, Y. Liu, M. Zheng, *Chem. Eng. J.* **2020**, *384*, 123266.
[26] J. Han, H. Lee, J. Kim, S. Kim, H. Kim, E. Kim, Y.-E. Sung, K. Kim, J.-C. Lee, *J. Membr. Sci.* **2020**, *612*, 118428.
[27] V. Dinca, Q. Liu, S. Brajnicov, A. Bonciu, A. Vlad, C. Z. Dinu, *Compos. Commun.* **2020**, *17*, 115.
[28] W. Li, Z. Xu, L. Chen, M. Shan, X. Tian, C. Yang, H. Lv, X. Qian, *Chem. Eng. J.* **2014**, *237*, 291.
[29] T. Xue, W. Fan, X. Zhang, X. Zhao, F. Yang, T. Liu, *Composites, Part B* **2021**, *219*, 108963.
[30] D. Xu, Y. Gao, Y. Sun, Z. Wang, Z. Jiang, X. Jiang, H. Zhang, *Macromol. Chem. Phys.* **2019**, *220*, 1800553.
[31] W. Tong, Y. Zhang, Q. Zhang, X. Luan, Y. Duan, S. Pan, F. Lv, Q. An, *Carbon* **2015**, *94*, 590.
[32] Y. Pang, J. Yang, T. Curtis, S. Luo, D. Huang, Z. Feng, J. O. Morales-Ferreiro, P. Sapkota, F. Lei, J. Zhang, Q. Zhang, E. Lee, Y. Huang, R. Guo, S. Ptasinska, R. K. Roeder, T. Luo, *ACS Nano* **2019**, *13*, 1097.
[33] X. Zhang, L. Wu, J. Wang, *Macromol. Chem. Phys.* **2018**, *219*, 1800161.
[34] J. Ji, J. Zhao, W. Guo, *J. Mech. Phys. Solids* **2019**, *128*, 79.
[35] Y. Matsushita, *Macromolecules* **2007**, *40*, 771.
[36] X. Zhang, J. Chen, L. Xu, T. Liu, *Chin. J. Polym. Sci.* **2021**. https://doi.org/10.1007/s10118-021-2591-2.
[37] S. Plimpton, *J. Comput. Phys.* **1995**, *117*, 1.
[38] T. Jiang, L. Wang, J. Lin, *RSC Adv.* **2014**, *4*, 35272.
[39] L. Zhang, J. Lin, S. Lin, *Soft Matter* **2009**, *5*, 173.
[40] X. Zhu, L. Wang, J. Lin, *Macromolecules* **2011**, *44*, 8314.
[41] C. J. Martinez, J. Liu, S. K. Rhodes, E. Luijten, E. R. Weeks, J. A. Lewis, *Langmuir* **2005**, *21*, 9978.
[42] G. D. Smith, D. Bedrov, *Langmuir* **2009**, *25*, 11239.
[43] B. Ma, X. Wang, Y. He, Z. Dong, X. Zhang, X. Chen, T. Liu, *Polymer* **2021**, *212*, 123280.
[44] J. Zhao, J.-W. Jiang, Y. Jia, W. Guo, T. Rabczuk, *Carbon* **2013**, *57*, 108.